# Characterization of Electrical Transitions Using Transmission Line Measurements

Reydezel Torres-Torres, *Member, IEEE*, Gaudencio Hernández-Sosa, *Student Member, IEEE*, Gerardo Romo, *Member, IEEE*, and Adan Sánchez, *Member, IEEE*

***Abstract*—An analytical methodology for characterizing electrical transitions associated with transmission line-based microwave channels is presented in this paper. The methodology is formulated using $ABCD$ matrixes obtained from $S$-parameters measured to two lines with different length and terminated with the transition under investigation. This allows to determine the two-port network parameters of the transition in a simple and direct way. Excellent results are obtained when characterizing coplanar waveguide-to-microstrip and coaxial-to-microstrip transitions. Moreover, the methodology was also successfully applied to obtain the network parameters of packages fabricated on printed circuit board technology.**

***Index Terms*—$ABCD$ matrix, electrical transitions, transmission lines.**

## I. Introduction

TRANSMISSION lines play a key role in electronic systems, particularly when the operation frequency is within the microwave range. In practice, these lines must be accurately characterized to assess the performance of the microwave circuits and systems, and to provide information to carry out interconnect optimization and preserve signal integrity. For this reason, several methods have been reported to characterize transmission line interconnects. However, these methods are only dedicated to obtain the fundamental parameters such as the complex propagation constant [1]–[3] and the characteristic impedance [4]–[7]. Nonetheless, in addition to these parameters, the characteristics of the electrical transitions related to an actual interconnect must be accurately obtained to assess their performance and to provide information for optimization purposes. These transitions can be associated either with the connectors and pads used to probe the microwave circuits, or with the impedance discontinuities occurring as the signals are propagated throughout a complex interconnection channel.

In recent years, several methods have been reported to extract the network parameters of electrical transitions. However, these methods often require full-wave simulations and parameter optimization to carry out a detailed characterization [8]–[11], which becomes increasingly difficult and time-inefficient for complex structures. Other approaches use equivalent circuit models to represent the transitions [12]–[14]. In this case, however, analytical parameter determination methods for circuit elements have not been reported. An alternative methodology for determining the network parameters of electrical discontinuities was reported in [15], where coaxial connectors are characterized directly from experimental data. The formulation of this method, however, uses $Z$-parameters, which is not the best choice when characterizing transmission line-based channels since it considerably complicates the calculation of the model parameters.

Thus, in order to overcome the drawbacks of previously reported methods, a simple and analytical methodology to characterize the electrical transitions occurring in a transmission line-based channel is presented. This methodology is formulated from the experimental voltage–current chain ($ABCD$) parameters of two transmission lines with different lengths and terminated with the discontinuity to be characterized. The new technique is applied to characterize typical discontinuities occurring in transmission lines fabricated on printed circuit board (PCB) technology, and excellent results are observed within the tens of GHz range.

Manuscript received February 28, 2008; revised June 09, 2008. First published January 09, 2009; current version published February 13, 2009. This work was supported in part by the Mexico Fed. Government Sec. de Economía, CONACyT, and COECyTJAL. This work was recommended for publication by Associate Editor M. Cases upon evaluation of the reviewers comments.

R. Torres-Torres and G. Hernández-Sosa are with the Department of Electronics, Instituto Nacional de Astrofísica, Óptica y Electrónica (INAOE), Tonantzintla, Puebla 72840, Mexico. (email: reydezel@inaoep.mx).

G. Romo and A. Sánchez are with the Intel Mexico Research Center, Tlaquepaque, Jalisco 45700, Mexico.

Digital Object Identifier 10.1109/TADVP.2008.2004631

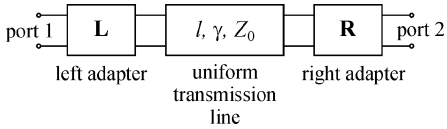


Fig. 1. Cascade model for a transmission line embedded between two electrical discontinuities.

## II. Formulation of the Characterization Method

Different types of transitions can be used to measure a two-port device under test (DUT) using a vector network analyzer (VNA). These transitions can be considered as propagation mode adapters that introduce discontinuities in the electrical path of the signal. Thus, an actual transmission line-based test structure can be represented by means of the block model of Fig. 1. In this case, a uniform transmission line (UTL) featuring a length $l$, a complex propagation constant $\gamma$, and a characteristic impedance $Z_0$ is considered to be embedded between two passive adapters. In accordance to this model, the matrix associated with the $ABCD$ parameters of this structure is given by

$$\mathbf{T}_{Xn} = \mathbf{L}\,\mathbf{T}_n\,\mathbf{R} \tag{1}$$

where $\mathbf{L}$ and $\mathbf{R}$ are the matrixes associated with the left and right adapters, respectively, $\mathbf{T}_n$ is the matrix of the UTL, and

the subscript $n$ is added to distinguish between the parameters of lines with different length used later. Thus, using transmission line theory, $\mathbf{T}_n$ can be expressed as [16]

$$\mathbf{T}_n = \begin{bmatrix} c_n & Z_0 s_n \\ Z_0^{-1} s_n & c_n \end{bmatrix} \tag{2}$$

where $c_n = \cosh(\gamma l_n)$ and $s_n = \sinh(\gamma l_n)$. Thus, since the complex values for $\gamma$ and $Z_0$ of the UTL can be determined using previously reported methods [2], [4], $\mathbf{T}_n$ can be easily obtained for a given line length.

For the case of the adapters, $\mathbf{L}$ and $\mathbf{R}$ are, respectively, expressed as

$$\mathbf{L} = \begin{bmatrix} \alpha & \beta \\ \delta & \varepsilon \end{bmatrix} \tag{3}$$

$$\mathbf{R} = \begin{bmatrix} \varepsilon & \beta \\ \delta & \alpha \end{bmatrix}. \tag{4}$$

Notice in (3) and (4) that the adapters are assumed to be identical and reciprocal, but one is rotated 180° with respect to the other.

At this point, it is necessary to mention that the electrical transitions represented by means of the adapters are fully characterized once $\alpha$, $\beta$, $\delta$, and $\varepsilon$ are determined. For this reason, a procedure to directly obtain $\mathbf{L}$ and $\mathbf{R}$ from the experimental $\mathbf{T}_{Xn}$ matrixes associated with two lines of different lengths is proposed hereafter.

Substituting (2)–(4) into (1) and simplifying yields

$$\mathbf{T}_{Xn} = \frac{1}{Z_0}\begin{bmatrix} A_n & B_n \\ C_n & D_n \end{bmatrix} = \frac{1}{Z_0}\begin{bmatrix} e\,c_n + f\,s_n & g\,c_n + h\,s_n \\ k\,c_n + m\,s_n & p\,c_n + q\,s_n \end{bmatrix} \tag{5}$$

where $g$ and $h$ are, respectively, given by

$$g = 2\,\alpha\,\beta\,Z_0 \tag{6}$$

$$h = \alpha^2\,Z_0^2 + \beta^2 \tag{7}$$

whereas $e$, $f$, $p$, and $q$ can also be easily written in terms of the adapter parameters and $Z_0$. These parameters, however, are not used in this formulation. For the case of $k$ and $m$, the corresponding defining equations are presented later in this section.

Continuing with the formulation, $g$ and $h$ can be determined from the experimental $ABCD$ parameters of two lines differing only in length and terminated with the same adapters. In this case, the corresponding $ABCD$ matrixes are named $\mathbf{T}_{X1}$ and $\mathbf{T}_{X2}$. By doing this, the unknowns in (6) and (7) are reduced to $\alpha$ and $\beta$.

In accordance to (5)

$$B_1 = g\,c_1 + h\,s_1 \tag{8}$$

$$B_2 = g\,c_2 + h\,s_2. \tag{9}$$

This is a linear equation system with two unknowns that can be solved for $g$ and $h$, which yields

$$g = \frac{B_1 s_2 - B_2 s_1}{\Delta} \tag{10}$$

$$h = \frac{B_2 c_1 - B_1 c_2}{\Delta} \tag{11}$$

where

$$\Delta = c_1 s_2 - c_2 s_1. \tag{12}$$

Once $g$ and $h$ are known, $\alpha$ and $\beta$ are determined by simultaneously solving (6) and (7). In this case, the following equations are obtained:

$$\beta^4 + \frac{g^2}{4} - h\beta^2 = 0 \tag{13}$$

$$\alpha = \frac{g}{2\,\beta\,Z_0}. \tag{14}$$

Hence, $\beta$ is obtained first by solving (13); then, $\alpha$ is calculated by applying (14). Notice that, in order to reduce computing time, (13) can be firstly solved for $\beta^2$ and then $\beta$ can be obtained by calculating the corresponding square root. The root selection for (13) is discussed in the following section.

In order to determine $\delta$ and $\varepsilon$, a similar procedure can be applied. In this case, however, the expressions that define $k$ and $m$ are used. These are

$$k = 2\,\delta\,\varepsilon\,Z_0 \tag{15}$$

$$m = \delta^2\,Z_0^2 + \varepsilon^2. \tag{16}$$

Thus, $k$ and $m$ have to be determined to reduce the unknowns in (15) and (16) to $\delta$ and $\varepsilon$. With this purpose, using the experimental data associated with two lines and similarly to the expressions (8), (9), an equation system associated with $C_n$ can be written; this is

$$C_1 = k\,c_1 + m\,s_1 \tag{17}$$

$$C_2 = k\,c_2 + m\,s_2. \tag{18}$$

Solving for $k$ and $m$ yields

$$k = \frac{C_1 s_2 - C_2 s_1}{\Delta} \tag{19}$$

$$m = \frac{C_2 c_1 - C_1 c_2}{\Delta}. \tag{20}$$

Afterwards, $\delta$ and $\varepsilon$ are obtained by simultaneously solving (15) and (16), yielding the following equations:

$$\varepsilon^4 + \frac{k^2}{4} - m\varepsilon^2 = 0 \tag{21}$$

$$\delta = \frac{k}{2\,\varepsilon\,Z_0}. \tag{22}$$

In consequence, $\varepsilon$ is determined by solving (21) and $\delta$ is directly calculated from (22). At this point, it has been shown that the adapter network parameters can be analytically determined from experimental $ABCD$ parameters of two transmission line-based test-structures differing only in length. In the following section, the criterion to select the correct root for (13) and (21) is discussed.

## III. Root Selection

There are four values for $\beta$ that satisfy (13), and the same applies for $\varepsilon$ and (21). This means that there are sixteen possible combinations of values that $\beta$ and $\varepsilon$ can take to define $\mathbf{L}$

and $\mathbf{R}$ matrixes. Fortunately, it is known that the adapters represented by these matrixes are passive devices that present reciprocity. Thus, the $ABCD$ matrixes associated with the left and right adapters necessarily have to satisfy the passivity condition which is verified by applying the following expressions:

$$|S_{11}|^2 + |S_{21}|^2 < 1 \tag{23}$$
$$|S_{22}|^2 + |S_{12}|^2 < 1 \tag{24}$$

where the subscripted $S$-parameters correspond to the two-port scattering parameters of the adapter.

In order to write (23) and (24) in terms of the $ABCD$ parameters of the adapter defined in (3) and (4), the corresponding two-port $S$-to-$ABCD$ parameter conversion can be applied. Thus, the passivity conditions can be expressed as

$$\left|\frac{X_1 - X_2}{X_1 + X_2}\right|^2 + \left|\frac{2}{X_1 + X_2}\right|^2 < 1 \tag{25}$$
$$\left|\frac{-X_1 + X_2 + X_3}{X_1 + X_2}\right|^2 + \left|\frac{2X_0}{X_1 + X_2}\right|^2 < 1 \tag{26}$$

where

$$X_0 = \alpha\varepsilon - \beta\delta \tag{27}$$
$$X_1 = \alpha + \beta \tag{28}$$
$$X_2 = \delta + \varepsilon \tag{29}$$
$$X_3 = 2(\beta - \delta) \tag{30}$$

and a reference impedance for the $S$-parameters of 1 $\Omega$ has been assumed for simplicity in this conversion.

A second useful criterion can be used to discriminate the roots of (13) and (21); this is reciprocity. In this case, the roots have to be selected so that

$$X_0 = 1. \tag{31}$$

The correct roots of (13) and (21) satisfy simultaneously the passivity and reciprocity conditions. In this case, the correct values for $\alpha$, $\beta$, $\delta$ and $\varepsilon$ satisfy (31). However, in accordance to (27), (31) can also be satisfied by the negative value of $\alpha$, $\beta$, $\delta$, and $\varepsilon$, which introduces a sign ambiguity for the adapter characterization solution. For this reason, one useful criterion to resolve this ambiguity is explained hereafter.

A reciprocal device can be represented by means of a T-network as the one shown in Fig. 2. Notice in this figure that $z_1$ and $z_2$ are assumed to be different since the adapter is not necessarily symmetrical. According to this T-network, the $ABCD$ matrix associated with $\mathbf{L}$ can be expressed as

$$\mathbf{L} = \begin{bmatrix} 1 + y\,z_1 & z_1 + z_2 + y\,z_1\,z_2 \\ y & 1 + y\,z_2 \end{bmatrix} \tag{32}$$

where $z_1$ and $z_2$ are the series impedances and $y$ is the shunt admittance. It is important to point out that independently of the effects associated with $z_1$, $z_2$, and $y$, these parameters present pure positive real numbers within the direct-current (dc) regime (i.e., in dc the reactance is zero). Thus, comparing (3) and (32) leads to the conclusion that $\alpha$, $\beta$, $\delta$, and $\varepsilon$ present a positive real part at low frequencies. This suggests that, at relatively low frequencies the sign ambiguity is resolved, and for higher frequencies it can be resolved by considering that the real and imaginary parts of $\alpha$, $\beta$, $\delta$, and $\varepsilon$ are continuous when plotted versus frequency.

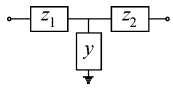


Fig. 2. T-network used to represent a reciprocal device.

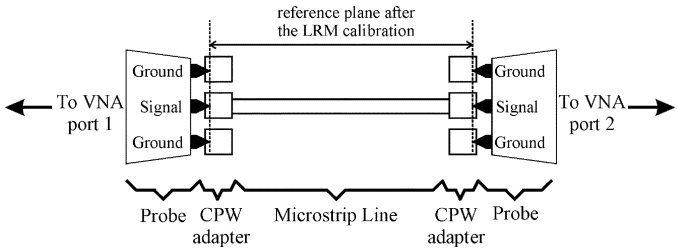


Fig. 3. Simplified sketch showing the reference plane for the experimental $S$-parameters once the VNA has been calibrated with the LRM procedure.

A final remark on the sign ambiguity solution is that, when $z_1$, $z_2$, and $y$ present low resistive components, the real part of $\beta$ and $\delta$ may be as low as the measurement resolution at low frequencies, complicating to determine if these parameters are negative or positive. Thus, the inspection of $\alpha$ and $\varepsilon$ at low frequencies is preferred when resolving the sign ambiguity.

## IV. Examples

### A. CPW-to-Microstrip Transition

CPW-to-microstrip (CPW-M) transitions designed to probe microstrip lines fabricated on PCB technology are characterized hereafter using the proposed method. With this purpose, microstrip lines of several lengths and terminated with CPW-M transitions were formed with copper over a substrate with nominal relative permittivity and loss tangent of 3.5 and 0.021, respectively. Afterwards, the $S$-parameters of these lines were measured from 0.1 to 30 GHz using a VNA and GSG coplanar probes with a pitch of 250 $\mu$m. The VNA system was previously calibrated up to the probe tips by using an impedance-standard-substrate (ISS) provided by the probe manufacturer and the line-reflect-match (LRM) procedure [17]. As can be seen in Fig. 3, once the system is calibrated the measurement reference plane is established at the outer edge of the CPW adapters, whereas the reference impedance for the experimental $S$-parameters is set at 50 $\Omega$. This step is required to obtain the $ABCD$ parameters of the lines from the $S$-parameters using the corresponding two-port network parameter conversion. Finally, in order to apply the proposed characterization method, $\gamma$ and $Z_0$ of the fabricated lines were determined as in [2] and [4], respectively.

Before applying the proposed method to the fabricated lines, the model for the CPW-M transition is briefly discussed. The equivalent circuit of Fig. 4 is based on the model proposed in

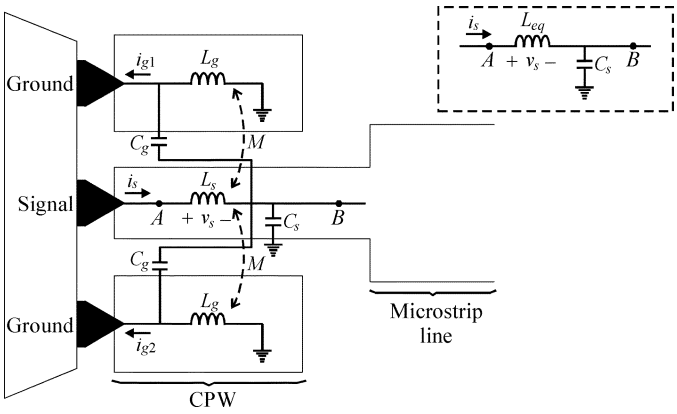


Fig. 4. Model for the CPW-M transition. Inset: simplified model.

[12] to represent a CPW-M transition. In this model, the currents at the pads are related by

$$i_s = i_{g1} + i_{g2} \tag{33}$$

where the sum $i_{g1} + i_{g2}$ represents the total current associated with the return path.

Since the pad capacitance is usually much bigger than the capacitance associated with the fringing effects (i.e., $C_s \gg C_g$), the voltage at the probe-to-signal pad interface can be approximated by

$$v_A = L_s \frac{di_s}{dt} - L_m \frac{di_{g1}}{dt} - L_m \frac{di_{g2}}{dt} + v_B \tag{34}$$

where $L_m$ is the mutual inductance. Thus, assuming $i_{g1} = i_{g2} = i_s/2$, (34) can be approximated by

$$v_A \approx L_{eq} \frac{di_s}{dt} + v_B \tag{35}$$

where

$$L_{eq} = L_s - L_m. \tag{36}$$

Thus, the CPW-M transition can be represented approximately by means of the equivalent circuit shown in the inset of Fig. 4. Notice that this circuit is a particular case of the model depicted in Fig. 2 with $y = j\omega C_s$, $z_1 = j\omega L_{eq}$, and $z_2 = 0$, being $\omega$ the angular frequency, and $j^2 = -1$.

Once that the model for the CPW-M transition has been analyzed, the characterization method was applied to the $ABCD$ matrixes corresponding to two 28-$\mu$m-wide lines with length ($l$) of 27.9 and 4.9 mm, respectively. Fig. 5 shows the experimentally determined $\alpha$ and $\varepsilon$ parameters for the CPW-M transition. As can be seen in this figure, $\alpha$ and $\varepsilon$ can be considered approximately as pure real numbers equal to 1 at least up to 30 GHz. Thus, after inspecting (3) and (32), it is concluded that in the analyzed transition the product between the shunt admittance and either one of the series impedances in the model of Fig. 2 is much less than 1 within the measured range plotted in Fig. 5. This observation allows the straightforward determination of the

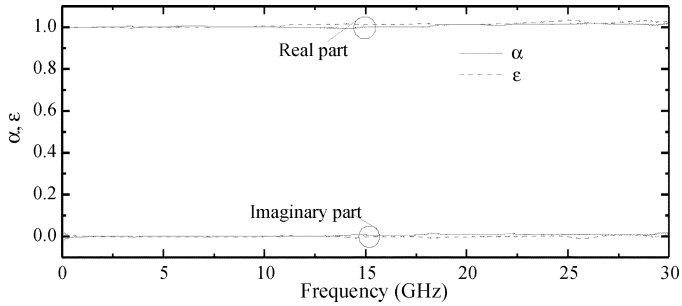


Fig. 5. Experimentally determined $\alpha$ and $\varepsilon$ parameters of the CPW-M adapter using the proposed methodology.

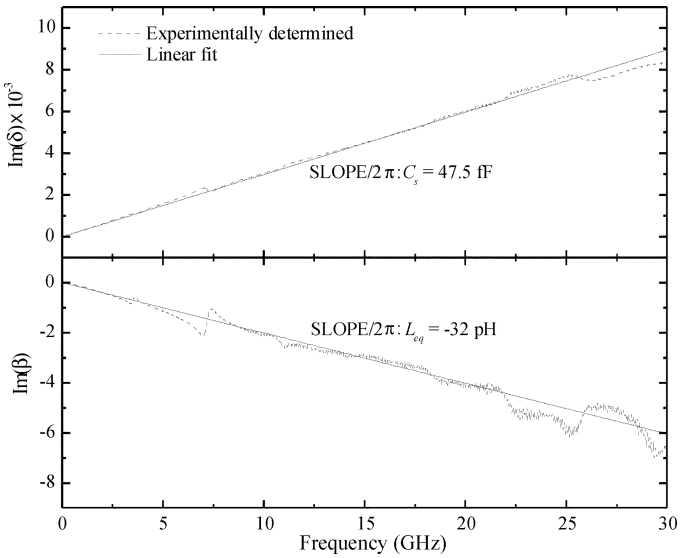


Fig. 6. Regression of experimentally determined data to obtain the equivalent circuit elements associated with the CPW-M transition.

equivalent circuit model parameters for this CPW-M transition as explained hereafter.

In order to determine the value of the series inductance and shunt capacitance in the simplified model of Fig. 4, $\beta$ and $\delta$ adapter parameters can be written in accordance to (32) as

$$\beta = j\omega L_{eq} \tag{37}$$

$$\delta = j\omega C_s. \tag{38}$$

Thus, $C_s$ and $L_{eq}$ can be determined from the slope of the linear regression of the $\mathrm{Im}(\delta)$ and $\mathrm{Im}(\beta)$ versus frequency curves respectively as shown in Fig. 6. Notice that the equivalent inductance seen at the edge of the CPW-M adapter is negative. According to (36), this indicates that the mutual inductance between the ground pads and the signal pad is bigger than the inductance of the signal pad. This effect of negative equivalent inductance has been studied previously in the literature [18].

After determining the experimental data associated with the CPW-M transition, the model of Fig. 1 was implemented for one of the characterized lines and the resulting simulation was compared with measured data in Fig. 7. Notice that excellent correlation between the simulated and measured return and insertion losses ($|S_{11}|$ and $|S_{21}|$, respectively) is observed. Moreover,

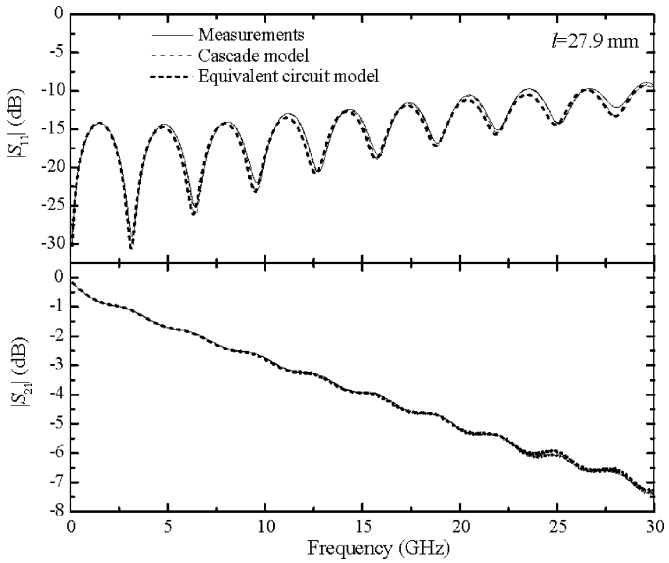


Fig. 7. Measured return and insertion losses compared with simulated data using a cascade and an equivalent circuit model for the line with $l = 27.9$ mm and terminated with CPW-M adapters.

when representing the transitions using the simplified model of Fig. 4 and the corresponding extracted values for $C_s$ and $L_{eq}$, also good agreement between simulated and experimental data is achieved as shown in Fig. 7.

### *B. Coaxial-to-Microstrip Transition*

In order to apply the characterization methodology to a coaxial-to-microstrip (CM) transition, $S$-parameters were measured to 150-$\mu$m-wide microstrip lines fabricated over a multilayer PCB made of FR4 material (nominal permittivity and loss tangent of 4.4 and 0.02, respectively). The lines are terminated with 1.85-mm female coaxial connectors and the separation between the lines and the ground plane (i.e., the substrate thickness) is 100 $\mu$m. As in the previous case, the VNA system was calibrated up to the beginning of the adapter to be characterized. In this case, however, the calibration was performed by using a coaxial calibration kit and the thru-reflect-line (TRL) procedure [1]. Thus, after performing the TRL calibration, the measurement reference plane is located as depicted in Fig. 8(a). Afterwards, the $S$-parameters of several coaxial-microstrip-coaxial channels were measured from 0.1 to 50 GHz and $\gamma$ and $Z_0$ were determined for the lines embedded between the CM transitions. A sketch of the CM transition to be characterized and its equivalent circuit is shown in Fig. 8(b) [19].

In accordance with the model of Fig. 1 and the equivalent circuit of Fig. 8(b), for the case of a CM transition the $ABCD$-matrix of the left adapter is written as

$$\mathbf{L} = \begin{bmatrix} \alpha & \beta \\ \delta & \varepsilon \end{bmatrix} = \begin{bmatrix} 1-\omega^2 C_2 L_c & j\omega L_c \\ j[\omega(C_1+C_2)-\omega^3 C_1 C_2 L_c] & 1-\omega^2 C_1 L_c \end{bmatrix}. \quad (39)$$

After determining $\alpha$, $\beta$, $\delta$, and $\varepsilon$ for the CM adapter by using the experimental $ABCD$-parameters of two lines with

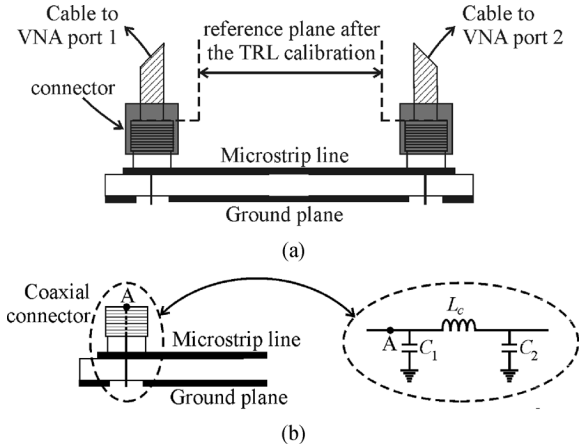


Fig. 8. (a) Simplified sketch showing the reference plane for the experimental S-parameters once the VNA has been calibrated with the TRL procedure. (b) Longitudinal view of the CM transition and the corresponding equivalent circuit model.

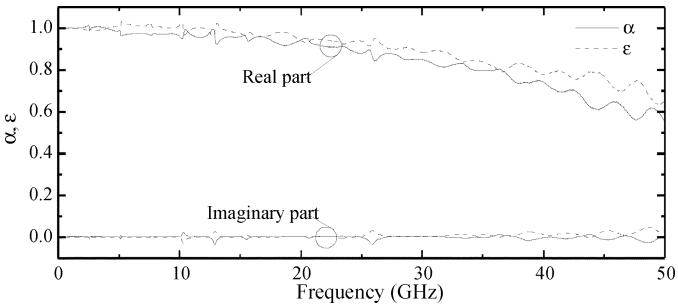


Fig. 9. Experimentally determined $\alpha$ and $\varepsilon$ parameters of the CM adapter using the proposed methodology.

$l = 58.4$ mm and $25.4$ mm, $\alpha$ and $\varepsilon$ were plotted versus frequency in Fig. 9. Notice that, as predicted by (39), the real parts of $\alpha$ and $\varepsilon$ decrease with frequency due to the fact that the products $\omega^2 C_1 L_c$ and $\omega^2 C_2 L_c$ become comparable to 1 within the measured frequency range for these transitions. Furthermore, the low value obtained for the corresponding imaginary parts shown in Fig. 9 are also in agreement with (39).

Continuing with the characterization of the CM adapter, the elements in the equivalent circuit of Fig. 8 can be obtained as explained hereafter.

After inspecting (39), $L_c$ can be determined from the slope of the linear regression of the $\mathrm{Im}(\beta)$ versus frequency curve as shown in Fig. 10. For the case of $C_1$ and $C_2$, two parameters can be defined from (36) to perform the corresponding extraction, these are

$$C_{x1} = \frac{1-\mathrm{Re}(\alpha)}{\omega \mathrm{Im}(\beta)} \quad (40)$$

$$C_{x2} = \frac{1-\mathrm{Re}(\varepsilon)}{\omega \mathrm{Im}(\beta)}. \quad (41)$$

Since $\mathrm{Re}(\alpha)$ and $\mathrm{Re}(\varepsilon)$ are approximately 1 at relatively low frequencies, the numerator in the right-hand side of (40) and (41) is small and the experimental data associated with these equations become noisy for small values of $\omega$. Thus, $C_1$ and $C_2$ are obtained, respectively, from a fit of the $C_{x1}$ and $C_{x2}$

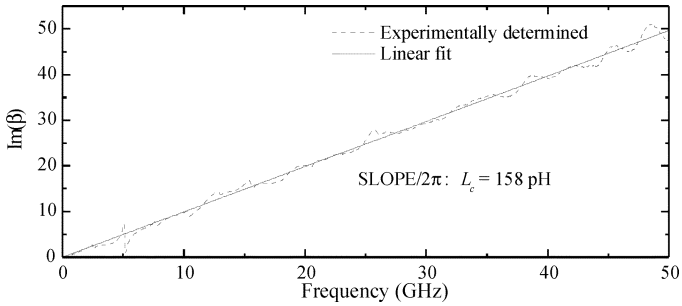


Fig. 10. Data regression to obtain $L_c$ for the CM transition.

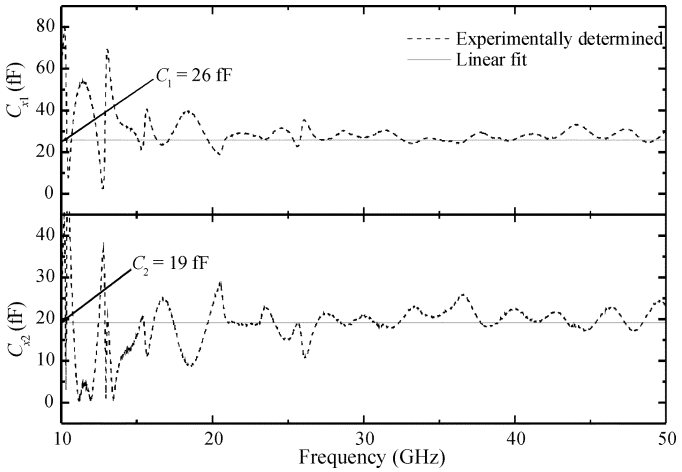


Fig. 11. Data regressions to obtain $C_1$ and $C_2$ for the CM transition.

versus frequency curves at a frequency range at which a plateau is observed. This extraction is illustrated in Fig. 11.

Once the experimental data associated with the CM adapters were obtained using the proposed methodology, the model of Fig. 1 was implemented and the corresponding simulations are compared with experimental data in Fig. 12. Good agreement between the simulated and the experimental return and insertion losses is observed even when representing the CM adapters by means of the model of Fig. 8.

### C. Characterization of an Electronic Package

In this case, a package designed to serve as a chip-to-PCB interface is characterized to demonstrate the application of the proposed methodology to analyze complex transitions. Thus, a procedure similar to that applied for the CPW adapters was followed. In this case, however, the implemented channel is shown in Fig. 13(a), whereas Fig. 13(b) shows the dimensions of the package used as transitional structure.

In order to carry out the characterization of the packages, two lines terminated with package transitions as the one shown in Fig. 13(a) were implemented. The lengths of the transmission lines separating the packages in each one of these structures are 24.5 and 76.2 mm, respectively. Afterwards, the $ABCD$-parameters of these structures were obtained from their corresponding $S$-parameters measured from 0.1 to 30 GHz using GSG probes. In this case, the probes were located at the top level of the packages and again the VNA system was calibrated up to the probe tips.

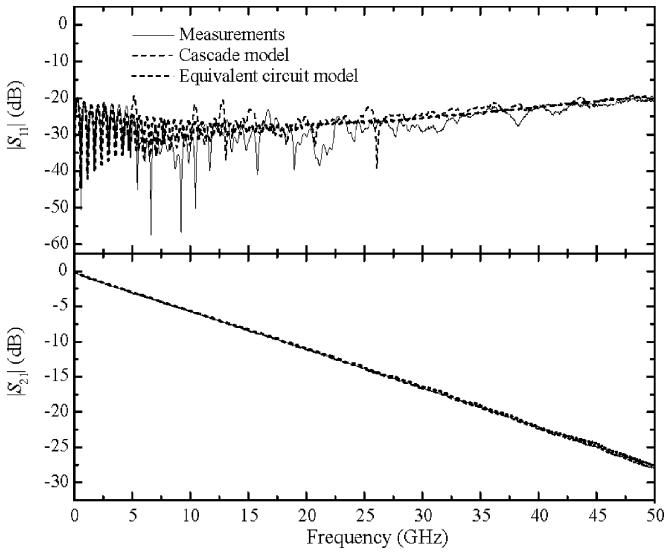


Fig. 12. Measured return and insertion losses compared with simulated data using a cascade and an equivalent circuit model for the line with $l = 141.8$ mm and terminated with female coaxial connectors.

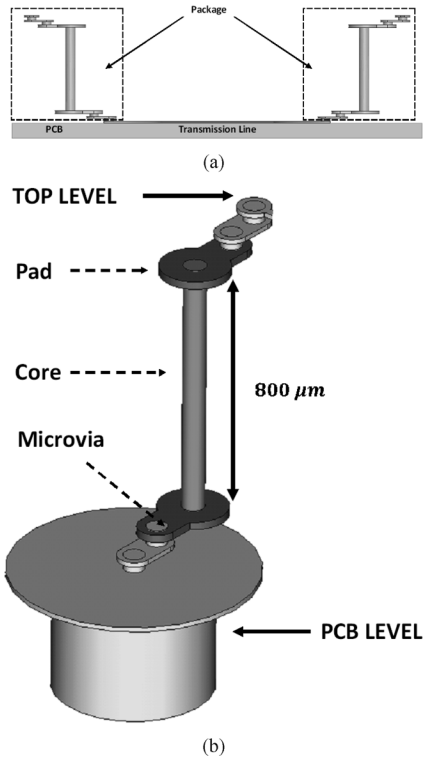


Fig. 13. (a) Cross-sectional view of a microstrip line terminated with package transitions. (b) The package transition in detail.

After determining the package parameters by using the proposed methodology, the corresponding return and insertion losses were plotted versus frequency in Fig. 14. In order to verify the validity of the experimentally determined data, these curves were compared with the data obtained by measuring directly the $S$-parameters associated with the package. In the latter case, a single package-to-microstrip transition (i.e., half of the channel shown in Fig. 13(a) was measured and the microstrip line at the bottom of the package was de-embedded

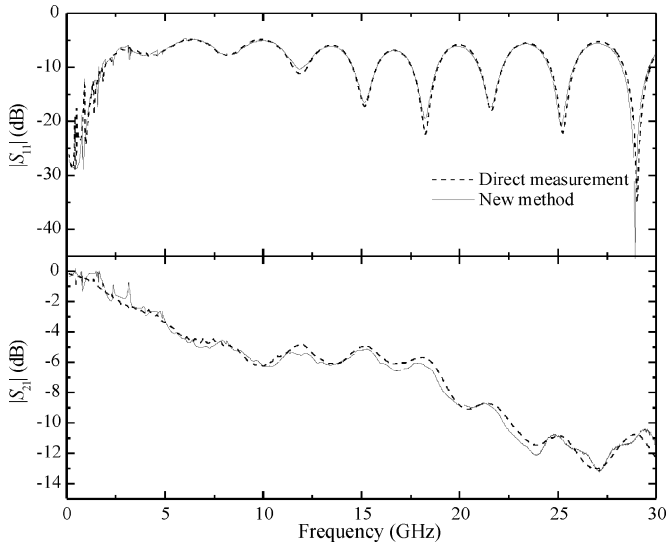


Fig. 14. Return and insertion losses for the characterized package obtained by applying the new method and by directly measuring the structure.

using a TRL calibration. Notice in Fig. 14 the excellent agreement between the data obtained with the new method and the measured data even though the curves correspond to a structure that was not used in the parameter determination process. This experiment was carried out to show the potential application of our characterization methodology to assess the performance of transitions with several electrical discontinuities using simple and conventional transmission-line based prototypes.

In addition, once that the $S$-parameters associated with the package are determined, further analysis can be carried out to infer the circuit topology required to represent this structure. Results in this direction have been reported in previous years [10], [20], [21]. However, general models and parameter extraction techniques for this type of transitions are still required due to the considerable variation of the structures depending on the application. In this case, applying the methodology proposed here represents a useful tool when developing these models and extraction techniques.

## V. Additional Considerations

In order to apply the proposed method, the measurement of two lines differing only in length and terminated with identical transitions is required to perform a simple and analytical parameter determination. However, it is necessary to bear in mind that the degree of repeatability of the transitions will have an impact on the accuracy of the determined parameters. This is due to the fact that in the formulation of the method $\alpha$, $\beta$, $\delta$, and $\varepsilon$ are assumed to remain invariable from transition to transition and from line to line. Thus, since the imperfections in actual transitions introduce variations in $\alpha$, $\beta$, $\delta$, and $\varepsilon$, special attention has to be paid when characterizing structures where the fabrication process tolerances may yield substantial variation in the electrical discontinuities from one structure to another, which is the case of some complex packages. Due to the impact of the transition variations in the accuracy of TRL-like de-embedding and characterization methods, measurements performed to multiple lines together with statistical analysis have been previously proposed to reduce the uncertainty in the results [22], which also may allow estimating the variations associated with imperfections in the transitions. Work in this direction is currently ongoing. Meanwhile, an appropriate and direct way to verify the validity of the extracted parameters for complex structures is reproducing the experimental data of a channel that includes the transition and that was not used in the parameter determination process.

A final remark in this section is the frequency range at which the method can be applied. As it was pointed out in the formulation of the method, $\gamma$ and $Z_0$ have to be known for the lines embedded between the transitions to be characterized. It is well known that the determination of these parameters is complicated at relatively low frequencies due to the impractically long lines required for the corresponding extraction. However, once these parameters are properly determined, the proposed method can be applied considering that as the physical dimensions of the transitions become smaller, the upper limit of the frequency range has to be increased. This is of especial importance to increase the resolution of the experimental data for implementing equivalent circuit models for transitions with small electrical discontinuities very close to each other.

## VI. Conclusion

An analytical methodology for characterizing electrical transitions occurring in transmission line based channels has been proposed and demonstrated. This methodology allows the direct determination of the $S$-parameters associated with the transitions from measurement performed to conventional test structures. The use of the approach described in this paper includes characterization of mode adapters used in transmission-line based test structures, and also the characterization of more complicated transitions such as packages. A simple but rigorous model parameter determination for two of the most common adapters used for microwave measurements on PCB was also carried out. In addition, the $S$-parameters for a package were obtained, which demonstrates that the proposed methodology can be a very useful tool when developing measurement-based models for electrical transitions.

## References

[1] G. F. Engen and C. A. Hoer, "Thru-reflect-line: An improved technique for calibrating the dual six-port automatic network analyzer," *IEEE Trans. Microw. Theory Tech.*, vol. 37, no. 12, pp. 987–993, Dec. 1979.

[2] J. A. Reynoso-Hernández, "Unified method for determining the complex propagation constant of reflecting and nonreflecting transmission lines," *IEEE Microwave Wireless Comp. Lett.*, vol. 13, no. 8, pp. 351–353, Aug. 2003.

[3] K. Narita and T. Kashta, "An accurate experimental method for characterizing transmission lines embedded in multilayer printed circuit boards," *IEEE Trans. Adv. Packag.*, vol. 29, no. 1, pp. 114–121, Feb. 2006.

[4] R. B. Marks and D. F. Williams, "Characteristic impedance determination using propagation constant measurement," *IEEE Microw. Guided Wave Lett.*, vol. 1, no. 6, pp. 141–143, Jun. 1991.

[5] D. F. Williams, U. Arz, and H. Grabinski, "Characteristic-impedance measurement error on lossy substrates," *IEEE Microwave Wireless Comp. Lett.*, vol. 11, no. 7, pp. 299–301, Jul. 2001.

[6] S. Vandenberghe, D. M. Schreurs, G. Carchon, B. K. Nauwelaers, and W. D. Raedt, "Characteristic impedance extraction using calibration comparison," *IEEE Trans. Microwave Theory Tech.*, vol. 49, no. 12, pp. 2573–2579, Dec. 2001.
[7] J. E. Post, "On determining the characteristic impedance of low-loss transmission lines," *Microwave Opt. Technol. Lett.*, vol. 47, pp. 176–180, Oct. 2005.
[8] G. Antonini, A. C. Scogna, and A. Orlandi, "S-parameters characterization of through, blind, and buried via holes," *IEEE Trans. Mobile Comput.*, vol. 2, pp. 174–184, Apr.–Jun. 2003.
[9] R. Araneo, "Extraction of broad-band passive lumped equivalent circuits of microwave discontinuities," *IEEE Trans. Microwave Theory Tech.*, vol. 54, no. 1, pp. 393–401, Jan. 2006.
[10] E. McGibney and J. Barrett, "An overview of electrical characterization techniques and theory for IC packages and interconnects," *IEEE Trans. Adv. Packag.*, vol. 29, no. 1, pp. 131–139, Feb. 2006.
[11] J. Lim, D. Kwon, J.-S. Rieh, S.-W. Kim, and S. Hwang, "RF characterization and modeling of various wire bond transitions," *IEEE Trans. Adv. Packag.*, vol. 28, no. 4, pp. 772–778, Nov. 2005.
[12] W. Wiatr, D. K. Walker, and D. F. Williams, "Coplanar-waveguide-to-microstrip transition model," in *IEEE MTT-S Int. Microw. Sym. Dig.*, Boston, MA, Jun. 2000, pp. 1797–1800.
[13] S. Luan, G. Selli, J. Fan, M. Lai, J. L. Knighten, N. W. Smith, R. Alexander, G. Antonini, A. Ciccomancini, A. Orlandi, and J. L. Drewniak, "SPICE model libraries for via transitions," in *IEEE Int. Symp. Electromagn. Compat. Dig.*, Boston, MA, Aug. 2003, pp. 859–864.
[14] D. Deslades and K. Wu, "Analysis and design of current probe transition from grounded coplanar to substrate integrated rectangular waveguides," *IEEE Trans. Microwave Theory Tech.*, vol. 53, no. 8, pp. 2487–2494, Aug. 2005.
[15] M. A. Goodberlet and J. B. Mead, "Microwave connector characterization," *IEEE Microw. Mag.*, vol. 7, no. 5, pp. 78–83, Oct. 2006.
[16] W. R. Eisenstadt and Y. Eo, "S-parameter-based IC interconnect transmission line characterization," *IEEE Trans. Compon., Hybrids, Manufact. Technol.*, vol. 15, no. 4, pp. 483–490, Aug. 1992.
[17] A. Davidson, K. Jones, and E. Strid, "LRM and LRRM calibrations with automatic determination of load inductance," in *Proc. 36th ARFTG Conf. Dig.*, Monterey, CA, Nov. 1990, pp. 57–63.
[18] D. S. Lymar, T. C. Neugebauer, and D. J. Perreault, "Coupled-magnetic filters with adaptive inductance cancellation," *IEEE Trans. Power Electron.*, vol. 21, no. 6, pp. 1524–1540, Nov.. 2003.
[19] D. M. Pozar, *Microwave Engineering*, 3rd ed. New York: Wiley, 2005.
[20] T. Horng, S. Wu, and C. Shih, "Complete methodology for electrical modeling of RFIC packages," *IEEE Trans. Adv. Packag.*, vol. 4, no. 4, pp. 542–547, Nov. 2001.
[21] Y. Kim, O. Kwon, and C. Lee, "Equivalent circuit extraction from the measured S-parameters of electronic packages," in *Proc. 6th Int. Conf. VLSI CAD*, Seoul, Korea, Oct. 1999, pp. 415–418.
[22] R. Marks, "A multiline method of network analyzer calibration," *IEEE Trans. Microwave Theory Tech.*, vol. 39, no. 7, pp. 1205–1215, Jul. 1991.

**Reydezel Torres-Torres** (S'01–M'06) was born in Mexico City, Mexico, in 1975. He received the B.S. degree in electrical engineering from the Instituto Tecnológico de Querétaro, Mexico, in 1998, and the M.S. and D.S. degrees in electronics from the Instituto Nacional de Astrofísica, Óptica y Electrónica (INAOE), Puebla, Mexico, in 2000 and 2003, respectively.

In 2001, he spent one year at IMEC, Leuven, Belgium, as part of his doctoral research project, working on the modeling and characterization of RF circuits and devices. From 2005 to 2006, he was with the Systems Research Center–Intel Mexico, where he carried out research on high-speed chip-to-chip PCB interconnects. Since 2007, he is a full-time researcher at the Electronics Department of INAOE and belongs to the National System of Researchers of Mexico.

**Gaudencio Hernández-Sosa** (S'08) was born in Mexico City, Mexico, in 1983. He received the B.S. degree in electronics from the Universidad Autónoma de Puebla, Mexico, in 2001, and the M.S. degree in electronics from the Instituto Nacional de Astrofísica, Óptica y Electrónica (INAOE), Puebla, Mexico, in 2008. He is currently working toward the D.S. degree in electronics at INAOE working on signal integrity aspects in chip-to-chip high-speed channels on printed circuit boards.

**Gerardo Romo** (S'02–M'05) was born in Jalisco, Mexico, in 1973. He received the B.S. degree in electronics from the Instituto Tecnológico de Aguascalientes, Mexico, in 1998, and the M.A.Sc. and Ph.D degrees in electrical engineering from Carleton University, Ottawa, ON, Canada, in 2001 and 2005, respectively.

He is currently with the Systems Research Center–Intel Mexico on research and development of high-speed interconnects and electronic packages.

**Adan Sánchez** (M'05) was born in Puebla, Mexico, in 1975. He received the B.S. degree in electronics from the Universidad Autónoma de Puebla, Mexico, in 1998, and the M.S. and D.S. degrees in electronics from the Instituto Nacional de Astrofísica, Óptica y Electrónica (INAOE), Puebla, Mexico, in 2000 and 2005, respectively. He is a Senior Hardware Engineer working on high-speed chip-to-chip PCB interconnects at the Systems Research Center–Intel Mexico.